Cancer Cell, Volume *15*

Supplemental Data

Article

Identification of CD15 as a Marker for Tumor-Propagating Cells in a Mouse Model of Medulloblastoma

Tracy-Ann Read, Marie P. Fogarty, Shirley L. Markant, Roger E. McLendon, Zhengzheng Wei, David W. Ellison, Phillip G. Febbo, and Robert J. Wechsler-Reya

Supplemental Experimental Procedures

Cell Isolation

GNPs were obtained from cerebella of 7-day-old WT mice, and tumor cells were obtained from 10- to 25-week-old *Ptc* and Math1-GFP/*Ptc*$^{+/-}$ mice displaying physical and behavioral signs of medulloblastoma. Cells were isolated as previously described (Oliver et al., 2005). Briefly, tumor tissue was digested in a solution containing 10 U/ml papain (Worthington, Lakewood, NJ) and 250 U/ml DNase (Sigma), and triturated to obtain a cell suspension. This suspension was centrifuged through a step gradient of 35% and 65% Percoll (Amersham Biosciences), and cells were harvested from the 35%-65% interface. Cells were resuspended in serum-free medium consisting of Neurobasal plus B27 supplement, sodium pyruvate, L-glutamine and penicillin/streptomycin (all from Invitrogen). Cells used for RNA isolation were centrifuged and flash frozen in liquid nitrogen. For proliferation assays cells were plated on poly-D-lysine (PDL)-coated tissue culture vessels and incubated in serum-free culture medium. To detect expression of surface markers by fluorescence-activated cell sorting (FACS), cells were resuspended in FACS buffer (Dulbecco's PBS + 5% FCS).

Flow Cytometry

To detect expression of surface markers, tumor cells were stained for 1 hour with primary antibodies, washed, stained for 30 minutes with secondary antibodies, and then analyzed or sorted using a FACS-Vantage SE flow cytometer (BD Biosciences, San Jose, CA).

For in vivo BrdU labeling studies, tumor bearing *Ptc*$^{+/-}$ mice were injected intraperitoneally with 200 µl of 10mg/ml BrdU. Two hours later tumor cells were harvested and fixed, permeabilized, DNase-treated and stained with anti-BrdU-APC antibodies using reagents from a BrdU Flow Kit (BD Pharmingen), following the manufacturer's protocol. Levels of cell-associated BrdU were analyzed using a FACS-Vantage SE flow cytometer.

Neurosphere Formation

Cells from P7 cerebellum and from *Ptc*$^{+/-}$ tumors were isolated as described above, and neurosphere cultures were initiated as described in (Lee et al., 2005). Briefly, unsorted cells or FACS-sorted CD133^{+} cells were cultured at clonal density (1000 cells/5ml) in Neurobasal medium with B27 supplement (NB-B27, Invitrogen) or in Neurocult medium with proliferation supplement (Stem Cell Technologies). Both types of culture medium were supplemented with 25 ng/ml bFGF (Invitrogen) and 25 ng/ml EGF (Peprotech). Cells were cultured for 10-40 days in uncoated dishes, and then photographed by bright-field

microscopy or stained for viability using a two-colored cell viability assay (Live/Dead Assay Kit, Invitrogen).

In Vivo Staining for CD15

Since our preliminary studies suggested that the CD15 epitope was sensitive to fixation and/or freezing, we labeled $CD15^+$ cells in vivo by injecting anti-CD15 secreting hybridoma cells into the forebrain, as previously described (Barres et al., 1992; Wechsler-Reya and Scott, 1999). Briefly**,** anti-CD15-secreting hybridoma cells (clone MMA, Catalog #HB-78) or isotype control hybridoma cells (clone 10E5, Catalog #HB-8513, both from American Type Culture Collection) were resuspended in serum-free medium containing 500 U/ml DNase at a density of 3×10^5 cells/µl. Cells were taken up in a 10 µl Hamilton syringe, and injected into Math1-GFP mice at P4 or into tumor bearing $Ptc^{+/-}$ or Math1-GFP/$Ptc^{+/-}$ mice at the first sign of symptoms. Cells were injected subpially, above the left frontal lobe, with 3 µl (approximately 1×10^6 cells). Three days after injection, mice were sacrificed, and cerebella were removed and fixed in 4% PFA. Cerebella were then sunk in 25% sucrose, frozen in O.C.T. and sectioned using a cryostat. Sections were post fixed with 4% PFA, blocked in PBS containing 2% BSA, 10% normal goat serum and 0.1% Triton X-100, and stained for 2 hours with Alexa Fluor-568-conguated goat-anti-mouse IgM (Invitrogen), and mounted with Fluoromount G. Samples were imaged and processed as described above.

Proliferation Assays

Tumor cells isolated as described above and resuspended in serum-free medium (Neurobasal + supplements) and transferred to PDL-coated 96-well plates, at a density of 2×10^5 cells/well. Cells were grown for 48h and pulsed with tritiated thymidine (methyl-[^{3}H]-Td, Amersham) and cultured for 14 hours. Following culture, cells were harvested onto filters using a Mach IIIM Manual Harvester 96 (Tomtec) and the amount of incorporated radioactivity was quantitated by liquid scintillation spectrophotometry using a Wallac MicroBeta microplate scintillation counter (Perkin Elmer).

RNA Isolation and Real-Time RT-PCR

To isolate total cytoplasmic RNA from GNPs and tumor cells, cell pellets were snap-frozen and RNA was isolated using the RNAqueous-Micro kit (Ambion), as described by the manufacturer. RNA was treated with DNase 1 (DNA-free, Ambion) to remove genomic DNA. RNA concentration was determined using the RiboGreen fluorescent dye (Molecular Probes) with a TD-700 fluorometer (Turner BioSystems). For real-time RT-PCR analysis, first-strand cDNA was synthesized using equivalent amounts of total RNA (0.1-1 µg) in a 20 µl reverse transcriptase reaction mixture (Invitrogen). Real-time PCR reactions were performed in triplicate using a 25 µl mixture containing iQ SYBR Green Supermix (BioRad), water, primers and 1 µl of cDNA. Gene-specific primers were used for *Nmyc*, *cyclin D1*, *Gli1, Ptc-1* (exons 2-3 and 7-9) *Tag-1, Ccnb1, Tle2, NeuroD1, Survivin, Hrk, L1-cam, Dcx and Notch2*; sequences for these are available upon request. Real-time quantitation was performed using the BIO-RAD iCycler iQ system (BioRad). Serial tenfold dilutions of cDNA were used as a reference for the standard curve calculation. Raw data were normalized based on expression of *actin*. In addition to real-time analysis, expression of *Ptc-1* exons 2-3 and 7-9 was also analyzed by conventional RT-PCR. Products were separated by electrophoresis on a 2% agarose gel and visualized after staining with ethidium bromide.

Microarray Preprocessing and $CD15^+$ Signature Development

A $CD15^+$ signature was developed by comparing microarray detected gene expression differences between tumor cells sorted for the absence of CD15 ($CD15^-$, n =6) or presence of CD15 ($CD15^+$, n =6) and using Bayesian methodologies for supervised learning as previously described (Bild et al., 2005; Huang et al., 2003; West et al., 2001). Specifically, samples used for the generation of the $CD15^+$ signature included the following:

Order	probeset_id	Class
1	Neuro-Wechsaffy-mouse-512645 CD15 - #5.CEL	0
2	Neuro-Wechsaffy-mouse-512645 CD15 - #7.CEL	0
3	Neuro-Wechsaffy-mouse-512645 CD15 -#10.CEL	0
4	Neuro-Wechsaffy-mouse-512645 CD15 -#12.CEL	0
5	Neuro-Wechsaffy-mouse-512645 CD15- #1.CEL	0
6	Neuro-Wechsaffy-mouse-512645 CD15- #3.CEL	0
7	Neuro-Wechsaffy-mouse-512645 CD15 + #11.CEL	1
8	Neuro-Wechsaffy-mouse-512645 CD15 + #2.CEL	1
9	Neuro-Wechsaffy-mouse-512645 CD15 + #4.CEL	1
10	Neuro-Wechsaffy-mouse-512645 CD15 + #6.CEL	1
11	Neuro-Wechsaffy-mouse-512645 CD15 + #8.CEL	1
12	Neuro-Wechsaffy-mouse-512645 CD15 + #9.CEL	1

Affymetrix data were pre-processed by using the standard methodology RMA (Bolstad et al., 2003; Irizarry et al., 2003), making a log2-transformation, and applying a filter to exclude the 10% of probe sets with the lowest variation in expression resulting in 40591 remaining features from the total number of 45101 features on the Mouse Genome 430 Plus 2 arrays. To identify differentially expressed genes, Student's t-tests were applied to the mean expression of samples after at least 12 hours of androgen exposure as compared to the mean expression of samples without androgen exposure. To control for the false discovery rate (FDR) of multiple tests, the Benjamini-Hochberg step-up procedure was applied to the nominal p-values (Benjamini and Hochberg, 1995).

The method for building a $CD15^+$ signature first identified a set of genes with the strongest levels of differential expression by CD15 expression status, as determined by t-tests (top 300 genes). A summary measure for the expression profile of the gene set, termed 'metagene', was derived from the top principle component of a singular value decomposition (SVD) (i.e. the linear combination of expression values that captures the most variance between phenotypes). A Bayesian probit regression model was used to build a predictive signature for the phenotypic differences. The determination of internal accuracy of the predictive signatures was assessed through proper leave-one-out cross-validation (see below), whereby the feature selection (i.e. metagene membership) is repeated for each iteration, and accuracy is determined according to a predictive probability ≥ 0.50 for each removed sample.

Proper Leave-One-Out Cross-Validation

Proper leave-one-out cross-validation is a method of analysis that tests for internal consistency of models derived from gene expression data. In leave-one-out cross-validation, starting with an original set of two classes or groups (e.g. a group of $CD15^+$ samples and a group of $CD15^-$ samples), one sample is removed and the remaining samples are used to develop a predictive model based on the differences between the two classes. The model generated is then applied to the left out sample to "guess" the identity of the sample. This is done, in turn, with each sample in the dataset. The accuracy and internal consistency of the model is judged based upon how well the "guessed" identity of the left out samples agrees with the known identities. The term "proper" refers to a method of leave-one-out cross-validation where the model is re-generated after each sample is left out. Earlier, less valid, forms of leave-one-out cross-validation generated a model using all samples, then left out single samples and applied the model generated on all samples to the left-out sample. This is less valid because information from the left-out sample was used to generate the model. This is a common method applied to models generated from complex data (for example, see (Singh et al., 2002)).

Development of a $CD15^+$ Signature

Mouse medulloblastomas were found to have a population of $CD15^+$ cells that could propagate tumors and a $CD15^-$ population that could not. Using recently developed computational methods we utilized

differentially expressed genes to create a "signature" of the $CD15^+$ tumor-propagating cell population. For all analyses, the $CD15^+$ signature was set at 300 genes and 1 metagene as this approximates the number of genes used in previously validated signatures (Bild et al., 2005; Potti et al., 2006).

Validation of the $CD15^+$ Signature

The $CD15^+$ signature was applied to an additional set of CD15 sorted medulloblastoma cells to validate that the $CD15^+$ signature could differentiate between two populations in an independent dataset. The files to which the $CD15^+$ signature was applied were as follows:

Order	Sample ID	CD15 Status
1	Neuro_Reya_affy_mouse_512645_Read_1.CEL	positive
2	Neuro_Reya_affy_mouse_512645_Read_2.CEL	neg
3	Neuro_Reya_affy_mouse_512645_Read_3.CEL	positive
4	Neuro_Reya_affy_mouse_512645_Read_4.CEL	neg
5	Neuro_Reya_affy_mouse_512645_Read_5.CEL	positive
6	Neuro_Reya_affy_mouse_512645_Read_6.CEL	neg
7	Neuro_Reya_affy_mouse_512645_Read_7.CEL	positive
8	Neuro_Reya_affy_mouse_512645_Read_8.CEL	neg
9	Neuro_Reya_affy_mouse_512645_Read_9.CEL	positive
10	Neuro_Reya_affy_mouse_512645_Read_10.CEL	neg

During the validation process, the original training samples used to develop the $CD15^+$ signature (n =12) were merged with the test samples (n =10) using Filemerger (http://tenero.duhs.duke.edu/genearray/perl/filemerger.pl) after expression values for each set were determined separately using RMA. Again, the same 10% filter was performed to exclude genes with minimal variation within the training samples. The $CD15^+$ signature was re-derived on the training samples and applied to each of the 10 test samples. This resulted in the assignment for each sample of a probability from 0 to 1 reflecting the similarity of the sample to the $CD15^+$ cells (perfect match would result in a probability of 1.0) compared to the $CD15^-$ cells (perfect match would result in a probability of 0.0). The results of each test sample is provided in the table below:

Order	Sample ID	CD15 Status	CD15+ Signature Probability
1	Neuro_Reya_affy_mouse_512645_Read_1.CEL	positive	0.73
2	Neuro_Reya_affy_mouse_512645_Read_2.CEL	neg	0.02
3	Neuro_Reya_affy_mouse_512645_Read_3.CEL	positive	0.95
4	Neuro_Reya_affy_mouse_512645_Read_4.CEL	neg	0.19
5	Neuro_Reya_affy_mouse_512645_Read_5.CEL	positive	0.96
6	Neuro_Reya_affy_mouse_512645_Read_6.CEL	neg	0.22
7	Neuro_Reya_affy_mouse_512645_Read_7.CEL	positive	0.92
8	Neuro_Reya_affy_mouse_512645_Read_8.CEL	neg	0.09
9	Neuro_Reya_affy_mouse_512645_Read_9.CEL	positive	0.89
10	Neuro_Reya_affy_mouse_512645_Read_10.CEL	neg	0.04

Application of the $CD15^+$ Signature

The $CD15^+$ was subsequently applied to two previously published datasets comprised of microarray data from human medulloblastoma tumors. As the $CD15^+$ signature was derived from murine cells on the Mouse microarrays, cross species and cross platform probe matching had to be performed. To accomplish this, an online resource developed at Duke was used called Chip Comparer (http://tenero.duhs.duke.edu/genearray/perl/chip/chipcomparer.pl). This allows users to find perfect match

probes between previously annotated arrays. The Mouse Genome 430 Plus 2 array was used as microarray A ("Mm:Mouse430_2") and the Affymetrix HuGene FL ("Hs:HuGeneFL") or the Affymetrix U133A version 2("Hs:HG_U133A_2") were used for the Pomeroy et al. and Thompson et al datasets, respectively, using primary UniGene cluster ID available from Affymetrix annotation file only ("primary locusID") and keeping multiple matches between the two platforms in separate rows ("in separate rows"). These ChipCompare files were then used together with the RMA processed files for the training samples and, separately each of the medulloblastoma datasets, to create single merged files using File Merger. All duplicate probes from either platform were removed after the files were merged and the remaining probe sets (n = 4748 for Pomeroy et al and n = 10745 for Thompson et al) were filtered to remove probes with minimal variation (probes with the lowest 10% Standard Deviation across training samples) (n = 4276 remaining for Pomeroy et al and n = 9671 for Thompson et al). These files were then used to re-derive the $CD15^{+}$ signature in the training samples from the mouse and apply the signature to each of the samples from both datasets as described above. Importantly, the same parameters were used to derive the signature: 300 genes and 1 metagene.

Supplemental References

Alabed, Y. Z., Pool, M., Ong Tone, S., and Fournier, A. E. (2007). Identification of CRMP4 as a convergent regulator of axon outgrowth inhibition. J Neurosci *27*, 1702-1711.

Allen, T., and Lobe, C. G. (1999). A comparison of Notch, Hes and Grg expression during murine embryonic and post-natal development. Cell Mol Biol (Noisy-le-grand) *45*, 687-708.

Altieri, D. C. (2003). Survivin and apoptosis control. Adv Cancer Res *88*, 31-52.

Baeriswyl, T., and Stoeckli, E. T. (2008). Axonin-1/TAG-1 is required for pathfinding of granule cell axons in the developing cerebellum. Neural Develop *3*, 7.

Barres, B. A., Hart, I. K., Coles, H. S., Burne, J. F., Voyvodic, J. T., Richardson, W. D., and Raff, M. C. (1992). Cell death and control of cell survival in the oligodendrocyte lineage. Cell *70*, 31-46.

Bellanger, S., de Gramont, A., and Sobczak-Thepot, J. (2007). Cyclin B2 suppresses mitotic failure and DNA re-replication in human somatic cells knocked down for both cyclins B1 and B2. Oncogene *26*, 7175-7184.

Benjamini, Y., and Hochberg, Y. (1995). Controlling the false discovery rate: a practical and powerful approach to multiple testing. J Royal Statistical Soc Series B *57*, 289-300.

Bild, A. H., Yao, G., Chang, J. T., Wang, Q., Potti, A., Chasse, D., Joshi, M. B., Harpole, D., Lancaster, J. M., Berchuck, A.*, et al.* (2005). Oncogenic pathway signatures in human cancers as a guide to targeted therapies. Nature.

Blanchard, J. M. (2000). Cyclin A2 transcriptional regulation: modulation of cell cycle control at the G1/S transition by peripheral cues. Biochem Pharmacol *60*, 1179-1184.

Bolstad, B. M., Irizarry, R. A., Astrand, M., and Speed, T. P. (2003). A comparison of normalization methods for high density oligonucleotide array data based on variance and bias. Bioinformatics (Oxford, England) *19*, 185-193.

Brandeis, M., Rosewell, I., Carrington, M., Crompton, T., Jacobs, M. A., Kirk, J., Gannon, J., and Hunt, T. (1998). Cyclin B2-null mice develop normally and are fertile whereas cyclin B1-null mice die in utero. Proceedings of the National Academy of Sciences of the United States of America *95*, 4344-4349.

Buscarlet, M., and Stifani, S. (2007). The 'Marx' of Groucho on development and disease. Trends Cell Biol *17*, 353-361.

Buttiglione, M., Revest, J. M., Pavlou, O., Karagogeos, D., Furley, A., Rougon, G., and Faivre-Sarrailh, C. (1998). A functional interaction between the neuronal adhesion molecules TAG-1 and F3 modulates neurite outgrowth and fasciculation of cerebellar granule cells. J Neurosci *18*, 6853-6870.

Chang, Y. F., Cheng, C. M., Chang, L. K., Jong, Y. J., and Yuo, C. Y. (2006). The F-box protein Fbxo7 interacts with human inhibitor of apoptosis protein cIAP1 and promotes cIAP1 ubiquitination. Biochem Biophys Res Commun *342*, 1022-1026.

Chapple, J. P., Anthony, K., Martin, T. R., Dev, A., Cooper, T. A., and Gallo, J. M. (2007). Expression, localization and tau exon 10 splicing activity of the brain RNA-binding protein TNRC4. Hum Mol Genet *16*, 2760-2769.

Cho, J. H., and Tsai, M. J. (2006). Preferential posterior cerebellum defect in BETA2/NeuroD1 knockout mice is the result of differential expression of BETA2/NeuroD1 along anterior-posterior axis. Developmental biology *290*, 125-138.

Crane, R., Gadea, B., Littlepage, L., Wu, H., and Ruderman, J. V. (2004). Aurora A, meiosis and mitosis. Biol Cell *96*, 215-229.

Daniels, R. H., Hall, P. S., and Bokoch, G. M. (1998). Membrane targeting of p21-activated kinase 1 (PAK1) induces neurite outgrowth from PC12 cells. Embo J *17*, 754-764.

Deconinck, A. E., Mead, P. E., Tevosian, S. G., Crispino, J. D., Katz, S. G., Zon, L. I., and Orkin, S. H. (2000). FOG acts as a repressor of red blood cell development in Xenopus. Development *127*, 2031-2040.

Deschenes-Furry, J., Perrone-Bizzozero, N., and Jasmin, B. J. (2006). The RNA-binding protein HuD: a regulator of neuronal differentiation, maintenance and plasticity. Bioessays *28*, 822-833.

Duncan, M. K., Bordas, L., Dicicco-Bloom, E., and Chada, K. K. (1997). Expression of the helix-loop-helix genes Id-1 and NSCL-1 during cerebellar development. Dev Dyn *208*, 107-114.

Fischer, G., Kunemund, V., and Schachner, M. (1986). Neurite outgrowth patterns in cerebellar microexplant cultures are affected by antibodies to the cell surface glycoprotein L1. J Neurosci *6*, 605-612.

Gout, I., Middleton, G., Adu, J., Ninkina, N. N., Drobot, L. B., Filonenko, V., Matsuka, G., Davies, A. M., Waterfield, M., and Buchman, V. L. (2000). Negative regulation of PI 3-kinase by Ruk, a novel adaptor protein. Embo J *19*, 4015-4025.

Huang, E., Ishida, S., Pittman, J., Dressman, H., Bild, A., Kloos, M., D'Amico, M., Pestell, R. G., West, M., and Nevins, J. R. (2003). Gene expression phenotypic models that predict the activity of oncogenic pathways. Nat Genet *34*, 226-230.

Huang, Y. S., Kan, M. C., Lin, C. L., and Richter, J. D. (2006). CPEB3 and CPEB4 in neurons: analysis of RNA-binding specificity and translational control of AMPA receptor GluR2 mRNA. Embo J *25*, 4865-4876.

Imhof, A., Schuierer, M., Werner, O., Moser, M., Roth, C., Bauer, R., and Buettner, R. (1999). Transcriptional regulation of the AP-2alpha promoter by BTEB-1 and AP-2rep, a novel wt-1/egr-related zinc finger repressor. Mol Cell Biol *19*, 194-204.

Irizarry, R. A., Bolstad, B. M., Collin, F., Cope, L. M., Hobbs, B., and Speed, T. P. (2003). Summaries of Affymetrix GeneChip probe level data. Nucleic acids research *31*, e15.

Jackson, R. S., 2nd, Cho, Y. J., Stein, S., and Liang, P. (2007). CYFIP2, a direct p53 target, is leptomycin-B sensitive. Cell cycle (Georgetown, Tex *6*, 95-103.

Kerjan, G., Dolan, J., Haumaitre, C., Schneider-Maunoury, S., Fujisawa, H., Mitchell, K. J., and Chedotal, A. (2005). The transmembrane semaphorin Sema6A controls cerebellar granule cell migration. Nat Neurosci *8*, 1516-1524.

Kiehl, T. R., Shibata, H., Vo, T., Huynh, D. P., and Pulst, S. M. (2001). Identification and expression of a mouse ortholog of A2BP1. Mamm Genome *12*, 595-601.

Koffa, M. D., Casanova, C. M., Santarella, R., Kocher, T., Wilm, M., and Mattaj, I. W. (2006). HURP is part of a Ran-dependent complex involved in spindle formation. Curr Biol *16*, 743-754.

Koizumi, H., Higginbotham, H., Poon, T., Tanaka, T., Brinkman, B. C., and Gleeson, J. G. (2006a). Doublecortin maintains bipolar shape and nuclear translocation during migration in the adult forebrain. Nat Neurosci *9*, 779-786.

Koizumi, H., Tanaka, T., and Gleeson, J. G. (2006b). Doublecortin-like kinase functions with doublecortin to mediate fiber tract decussation and neuronal migration. Neuron *49*, 55-66.

Kuan, C. Y., Whitmarsh, A. J., Yang, D. D., Liao, G., Schloemer, A. J., Dong, C., Bao, J., Banasiak, K. J., Haddad, G. G., Flavell, R. A., *et al.* (2003). A critical role of neural-specific JNK3 for ischemic apoptosis. Proceedings of the National Academy of Sciences of the United States of America *100*, 15184-15189.

Kuroda, Y., Oma, Y., Nishimori, K., Ohta, T., and Harata, M. (2002). Brain-specific expression of the nuclear actin-related protein ArpNalpha and its involvement in mammalian SWI/SNF chromatin remodeling complex. Biochem Biophys Res Commun *299*, 328-334.

Ladd, A. N., Charlet, N., and Cooper, T. A. (2001). The CELF family of RNA binding proteins is implicated in cell-specific and developmentally regulated alternative splicing. Mol Cell Biol *21*, 1285-1296.

Laman, H., Funes, J. M., Ye, H., Henderson, S., Galinanes-Garcia, L., Hara, E., Knowles, P., McDonald, N., and Boshoff, C. (2005). Transforming activity of Fbxo7 is mediated specifically through regulation of cyclin D/cdk6. Embo J *24*, 3104-3116.

Laub, F., Aldabe, R., Friedrich, V., Jr., Ohnishi, S., Yoshida, T., and Ramirez, F. (2001). Developmental expression of mouse Kruppel-like transcription factor KLF7 suggests a potential role in neurogenesis. Developmental biology *233*, 305-318.

Lee, A., Kessler, J. D., Read, T. A., Kaiser, C., Corbeil, D., Huttner, W. B., Johnson, J. E., and Wechsler-Reya, R. J. (2005). Isolation of neural stem cells from the postnatal cerebellum. Nat Neurosci *8*, 723-729.

Lessard, J., Wu, J. I., Ranish, J. A., Wan, M., Winslow, M. M., Staahl, B. T., Wu, H., Aebersold, R., Graef, I. A., and Crabtree, G. R. (2007). An essential switch in subunit composition of a chromatin remodeling complex during neural development. Neuron *55*, 201-215.

Li, C. M., Yan, R. T., and Wang, S. Z. (1999). Misexpression of a bHLH gene, cNSCL1, results in abnormal brain development. Dev Dyn *215*, 238-247.

Lindner, J., Rathjen, F. G., and Schachner, M. (1983). L1 mono- and polyclonal antibodies modify cell migration in early postnatal mouse cerebellum. Nature *305*, 427-430.

Lu, J. R., McKinsey, T. A., Xu, H., Wang, D. Z., Richardson, J. A., and Olson, E. N. (1999). FOG-2, a heart- and brain-enriched cofactor for GATA transcription factors. Mol Cell Biol *19*, 4495-4502.

Lu, Q., Sun, E. E., Klein, R. S., and Flanagan, J. G. (2001). Ephrin-B reverse signaling is mediated by a novel PDZ-RGS protein and selectively inhibits G protein-coupled chemoattraction. Cell *105*, 69-79.

Ma, C., Ying, C., Yuan, Z., Song, B., Li, D., Liu, Y., Lai, B., Li, W., Chen, R., Ching, Y. P., and Li, M. (2007). dp5/HRK is a c-Jun target gene and required for apoptosis induced by potassium deprivation in cerebellar granule neurons. J Biol Chem *282*, 30901-30909.

Meins, M., Schlickum, S., Wilhelm, C., Missbach, J., Yadav, S., Glaser, B., Grzmil, M., Burfeind, P., and Laccone, F. (2002). Identification and characterization of murine Brunol4, a new member of the elav/bruno family. Cytogenet Genome Res *97*, 254-260.

Miyata, T., Maeda, T., and Lee, J. E. (1999). NeuroD is required for differentiation of the granule cells in the cerebellum and hippocampus. Genes & development *13*, 1647-1652.

Nagy, J. I., Hacking, J., Frankenstein, U. N., and Turley, E. A. (1995). Requirement of the hyaluronan receptor RHAMM in neurite extension and motility as demonstrated in primary neurons and neuronal cell lines. J Neurosci *15*, 241-252.

Nagy, J. I., Price, M. L., Staines, W. A., Lynn, B. D., and Granholm, A. C. (1998). The hyaluronan receptor RHAMM in noradrenergic fibers contributes to axon growth capacity of locus coeruleus neurons in an intraocular transplant model. Neuroscience *86*, 241-255.

Nakakura, E. K., Watkins, D. N., Schuebel, K. E., Sriuranpong, V., Borges, M. W., Nelkin, B. D., and Ball, D. W. (2001). Mammalian Scratch: a neural-specific Snail family transcriptional repressor. Proceedings of the National Academy of Sciences of the United States of America *98*, 4010-4015.

Nakata, H., and Kozasa, T. (2005). Functional characterization of Galphao signaling through G protein-regulated inducer of neurite outgrowth 1. Mol Pharmacol *67*, 695-702.

Ohshima, T., Gilmore, E. C., Longenecker, G., Jacobowitz, D. M., Brady, R. O., Herrup, K., and Kulkarni, A. B. (1999). Migration defects of cdk5(-/-) neurons in the developing cerebellum is cell autonomous. J Neurosci *19*, 6017-6026.

Okamoto, Y., Ozaki, T., Miyazaki, K., Aoyama, M., Miyazaki, M., and Nakagawara, A. (2003). UbcH10 is the cancer-related E2 ubiquitin-conjugating enzyme. Cancer research *63*, 4167-4173.

Oliver, T. G., Read, T. A., Kessler, J. D., Mehmeti, A., Wells, J. F., Huynh, T. T., Lin, S. M., and Wechsler-Reya, R. J. (2005). Loss of patched and disruption of granule cell development in a pre-neoplastic stage of medulloblastoma. Development *132*, 2425-2439.

Oma, Y., Nishimori, K., and Harata, M. (2003). The brain-specific actin-related protein ArpN alpha interacts with the transcriptional co-repressor CtBP. Biochem Biophys Res Commun *301*, 521-528.

Paglini, G., Pigino, G., Kunda, P., Morfini, G., Maccioni, R., Quiroga, S., Ferreira, A., and Caceres, A. (1998). Evidence for the participation of the neuron-specific CDK5 activator P35 during laminin-enhanced axonal growth. J Neurosci *18*, 9858-9869.

Petronczki, M., Lenart, P., and Peters, J. M. (2008). Polo on the Rise-from Mitotic Entry to Cytokinesis with Plk1. Dev Cell *14*, 646-659.

Potti, A., Dressman, H. K., Bild, A., Riedel, R. F., Chan, G., Sayer, R., Cragun, J., Cottrill, H., Kelley, M. J., Petersen, R.*, et al.* (2006). Genomic signatures to guide the use of chemotherapeutics. Nat Med *12*, 1294-1300.

Rape, M., and Kirschner, M. W. (2004). Autonomous regulation of the anaphase-promoting complex couples mitosis to S-phase entry. Nature *432*, 588-595.

Renaud, J., Kerjan, G., Sumita, I., Zagar, Y., Georget, V., Kim, D., Fouquet, C., Suda, K., Sanbo, M., Suto, F.*, et al.* (2008). Plexin-A2 and its ligand, Sema6A, control nucleus-centrosome coupling in migrating granule cells. Nat Neurosci *11*, 440-449.

Sakurai, T., Lustig, M., Babiarz, J., Furley, A. J., Tait, S., Brophy, P. J., Brown, S. A., Brown, L. Y., Mason, C. A., and Grumet, M. (2001). Overlapping functions of the cell adhesion molecules Nr-CAM and L1 in cerebellar granule cell development. J Cell Biol *154*, 1259-1273.

Schmid, R. S., Midkiff, B. R., Kedar, V. P., and Maness, P. F. (2004). Adhesion molecule L1 stimulates neuronal migration through Vav2-Pak1 signaling. Neuroreport *15*, 2791-2794.

Singh, D., Febbo, P. G., Ross, K., Jackson, D. G., Manola, J., Ladd, C., Tamayo, P., Renshaw, A. A., D'Amico, A. V., Richie, J. P.*, et al.* (2002). Gene expression correlates of clinical prostate cancer behavior. Cancer cell *1*, 203-209.

Solecki, D. J., Liu, X. L., Tomoda, T., Fang, Y., and Hatten, M. E. (2001). Activated Notch2 signaling inhibits differentiation of cerebellar granule neuron precursors by maintaining proliferation. Neuron *31*, 557-568.

Steller, U., Kohls, S., Muller, B., Soller, R., Muller, R., Schlender, J., and Blohm, D. H. (1996). The RNA binding protein HuD: rat cDNA and analysis of the alternative spliced mRNA in neuronal differentiating cell lines P19 and PC12. Brain Res Mol Brain Res *35*, 285-296.

Takizawa, C. G., and Morgan, D. O. (2000). Control of mitosis by changes in the subcellular location of cyclin-B1-Cdk1 and Cdc25C. Curr Opin Cell Biol *12*, 658-665.

Verdaguer, E., Alvira, D., Jimenez, A., Rimbau, V., Camins, A., and Pallas, M. (2005). Inhibition of the cdk5/MEF2 pathway is involved in the antiapoptotic properties of calpain inhibitors in cerebellar neurons. Br J Pharmacol *145*, 1103-1111.

Wechsler-Reya, R. J., and Scott, M. P. (1999). Control of neuronal precursor proliferation in the cerebellum by Sonic Hedgehog [see comments]. Neuron *22*, 103-114.

West, M., Blanchette, C., Dressman, H., Huang, E., Ishida, S., Spang, R., Zuzan, H., Olson, J. A., Jr., Marks, J. R., and Nevins, J. R. (2001). Predicting the clinical status of human breast cancer by using gene expression profiles. Proceedings of the National Academy of Sciences of the United States of America *98*, 11462-11467.

Wheatley, S. P., and McNeish, I. A. (2005). Survivin: a protein with dual roles in mitosis and apoptosis. Int Rev Cytol *247*, 35-88.

Wong, J., and Fang, G. (2006). HURP controls spindle dynamics to promote proper interkinetochore tension and efficient kinetochore capture. J Cell Biol *173*, 879-891.

Xie, Q., Lin, T., Zhang, Y., Zheng, J., and Bonanno, J. A. (2005a). Molecular cloning and characterization of a human AIF-like gene with ability to induce apoptosis. J Biol Chem *280*, 19673-19681.

Xie, S., Xie, B., Lee, M. Y., and Dai, W. (2005b). Regulation of cell cycle checkpoints by polo-like kinases. Oncogene *24*, 277-286.

Xie, Y., Liu, Y., Ma, C., Yuan, Z., Wang, W., Zhu, Z., Gao, G., Liu, X., Yuan, H., Chen, R., *et al.* (2004). Indirubin-3'-oxime inhibits c-Jun NH2-terminal kinase: anti-apoptotic effect in cerebellar granule neurons. Neurosci Lett *367*, 355-359.

Yacubova, E., and Komuro, H. (2003). Cellular and molecular mechanisms of cerebellar granule cell migration. Cell Biochem Biophys *37*, 213-234.

Zhou, H. L., Baraniak, A. P., and Lou, H. (2007). Role for Fox-1/Fox-2 in mediating the neuronal pathway of calcitonin/calcitonin gene-related peptide alternative RNA processing. Mol Cell Biol *27*, 830-841.

A

Marker	Reported Expression	Expression Range (%)
A2B5	Neural & glial progenitors	0-60
PSA-NCAM	Neural progenitors	0-33
CD24	Neural Progenitors	0-10
CD44	Neural & glial progenitors	0-16
Sca-1	Stem Cells	0-4
CD117/c-kit	Stem Cells	0-3
CD57/HNK-1	Neural progenitors	7-88
R24/GD3	Neural & glial progenitors	1-8
CD15	Stem Cells & Progenitors	3-87

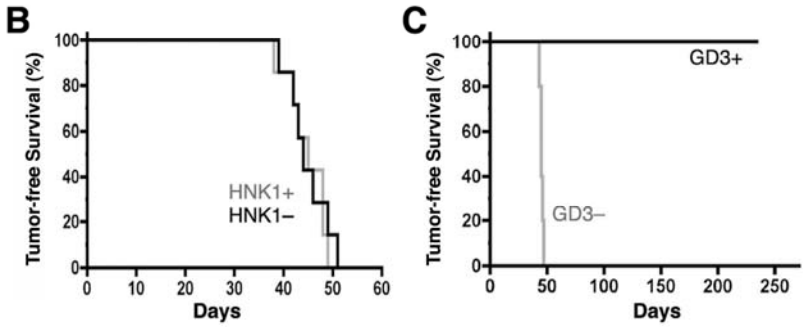

Figure S1. Screening for Markers that Enrich for Tumor-Propagating Cells

(A) Antibodies directed against the indicated cell surface antigens were used to stain tumor cells from *Ptc*$^{+/-}$ mice, and the percentage of positive and negative cells was determined. The majority of markers were not consistently expressed and were excluded from further analysis. Three markers – HNK1, GD3 and CD15 – were found in all tumors examined, and were tested to determine if they could be used to enrich for tumor-propagating cells by stereotaxic implantation into the cerebellum of SCID-beige mice.

(B) Tumors developed with similar frequency in animals that received HNK1^{+} and HNK1– cells, indicating that this marker could not be used for enrichment.

(C) Animals transplanted with GD3^{+} cells did not develop tumors, whereas those transplanted with GD3^{-} cells did. However, since 92-99% of tumor cells lack GD3, selecting for GD3^{-} cells did not result in substantial enrichment of the tumor-propagating population.

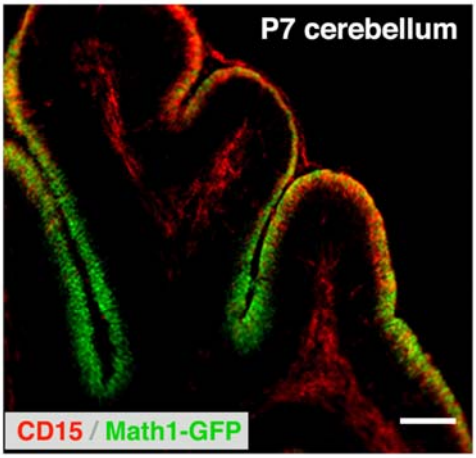

Figure S2. Expression of CD15 in the Neonatal Cerebellum

Math1-GFP neonates were injected intracranially with anti-CD15-secreting hybridomas to label $CD15^+$ cells in vivo (see Experimental Procedures for details). Cerebella were then sectioned and stained with fluorescently conjugated secondary antibodies to detect cells that had bound the anti-CD15 antibody (red) and with anti-GFP antibodies to label Math1-expressing cells (green). Note the expression of CD15 in the white matter as well as in a subset of GFP^+ cells in the external granule layer. Scale bar = 200 μm.

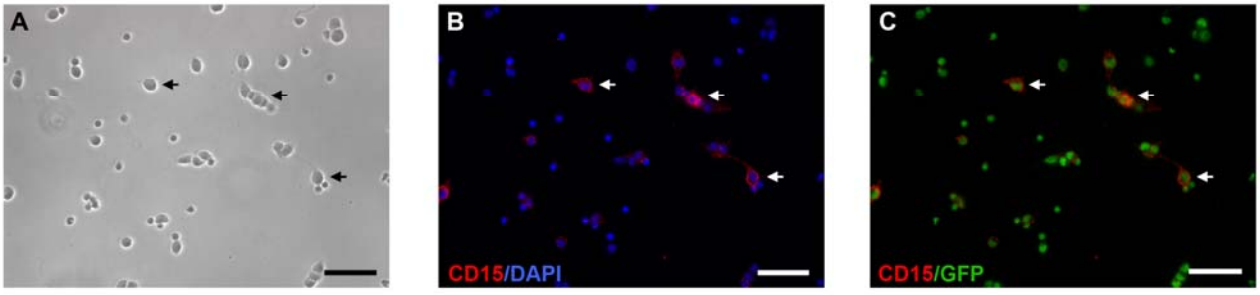

Figure S3. CD15 Staining of Tumor Cells

Tumor cells from Math1-GFP/*Ptc*$^{+/-}$ mice were cultured on poly-D-lysine coated coverslips for 6 hours, and stained with anti-CD15 antibodies and Alexa Fluor 568 secondary antibodies and DAPI.

(A) Phase contrast image of tumor cells.

(B and C) Cells from the same field, showing CD15 fluorescence (red) overlaid with DAPI (blue in B) or GFP (green in C). Arrows indicate three representative $CD15^+$ cells. Note that the majority of cells in the culture express GFP and that all $CD15^+$ cells are GFP^+. Scale bars = 50 μm.

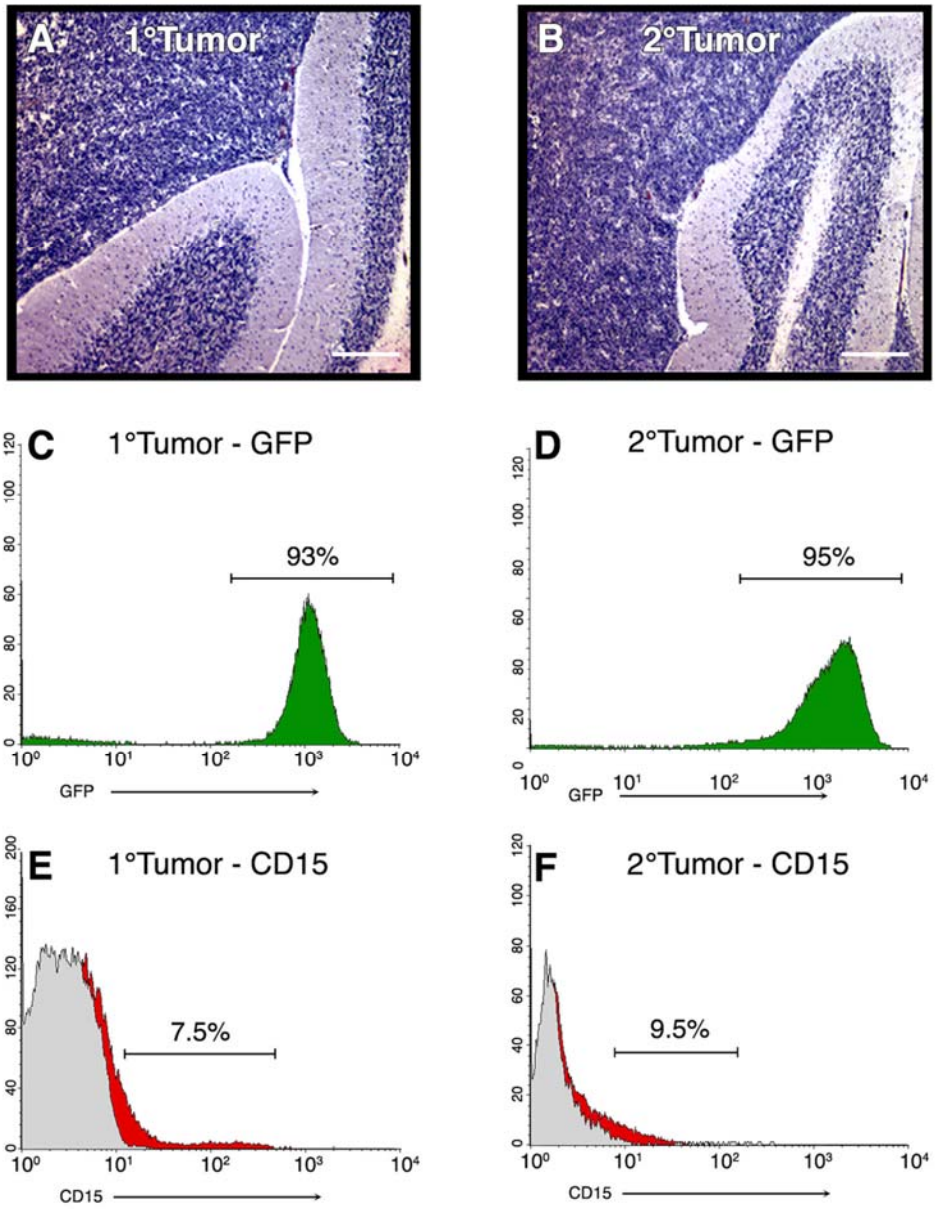

Figure S4. CD15^{+} Cells Recapitulate the Heterogeneity of *Ptc*$^{+/-}$ Tumors

Tumors from Math1-GFP/*Ptc*$^{+/-}$ mice were FACS sorted into CD15^{+} and CD15^{-} fractions and transplanted into SCID-beige mice.

(A and B) Sections from primary (A) and secondary (B) tumors were stained with H&E and examined by bright-field microscopy. Note the preponderance of small, densely-packed cells and the sharp tumor-normal tissue boundary in both primary and secondary tumors.

(C-F) FACS analysis. Cells from primary (C, E) and secondary (D and F) tumors were analyzed for expression of GFP (C and D) or stained with anti-CD15 antibodies (red histograms) or isotype-matched control antibodies (gray histograms) and analyzed by flow cytometry. The percentages of GFP^{+} and CD15^{+} cells (indicated above each histogram) are similar in primary and secondary tumors; thus CD15^{+} cells are capable of generating both CD15^{+} and CD15^{-} cells following transplantation. Scale bar = 100 μm.

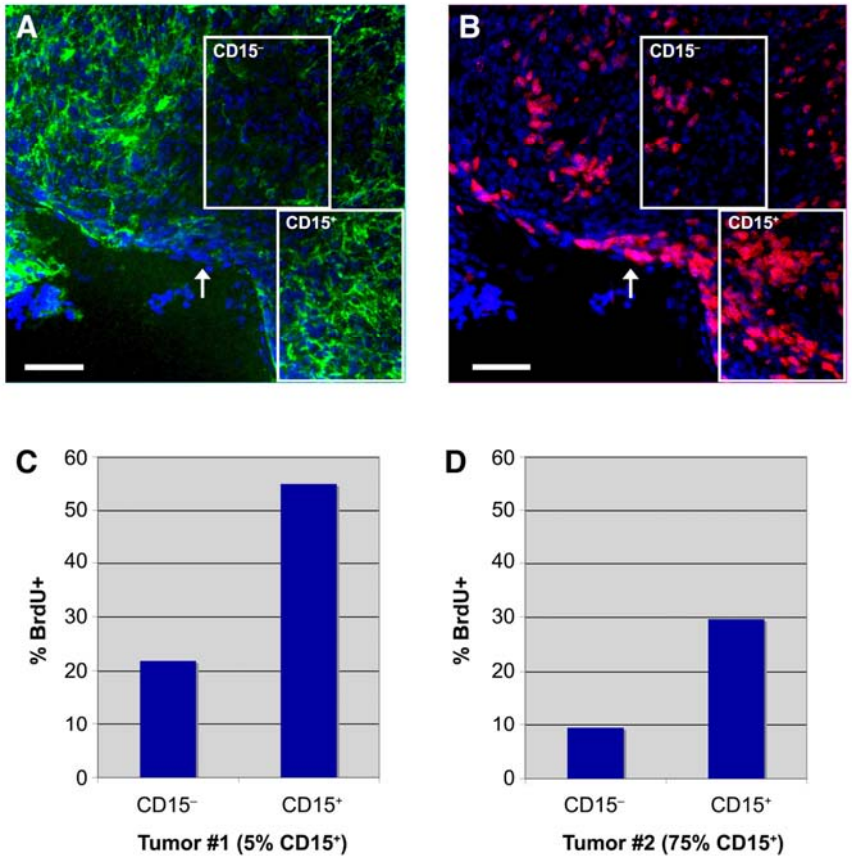

Figure S5. CD15$^+$ Tumor Cells Show Increased Proliferation In Vivo

(A and B) Immunofluorescence analysis. Tumor-bearing *Ptc*$^{+/-}$ mice were pulsed with BrdU, and 2 hours later, cerebellar sections were harvested, fixed and stained with anti-CD15 antibodies (green, A), anti-BrdU antibodies (red, B) and DAPI (blue). Regions with abundant CD15 staining frequently contain many BrdU$^+$ cells (lower boxes), whereas regions containing little CD15 staining contain fewer BrdU$^+$ cells (upper boxes). The correlation between CD15 and proliferation is not absolute, as regions lacking CD15 may also contain BrdU$^+$ cells (arrows).

(C and D) FACS analysis. Tumor-bearing *Ptc*$^{+/-}$ mice were pulsed with BrdU, and 2 hours later cells were harvested and stained with anti-CD15 and anti-BrdU antibodies. The proportion of CD15$^+$ and CD15$^-$ cells labeled with BrdU was quantitated by flow cytometry. Regardless of the abundance of CD15$^+$ cells in the tumor (5% in C, 75% in D), the CD15$^+$ population contained 2-3-fold more BrdU$^+$ cells than the CD15$^-$ population. Scale bars = 100 μm.

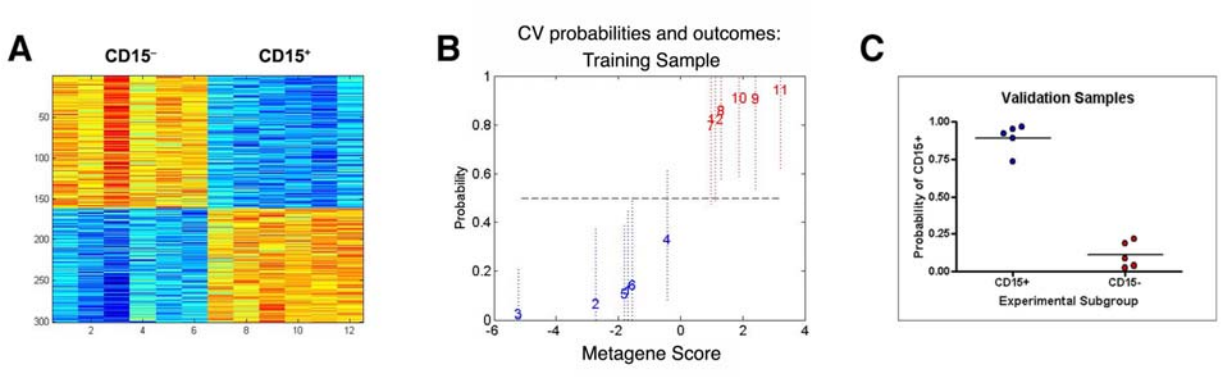

Figure S6. Development and Validation of the CD15$^+$ Gene Signature

(A) The top 300 genes with differential expression between CD15$^+$ and CD15$^-$ cell populations used to develop the CD15$^+$ signature. Individual genes are in rows, samples are in columns. Gene expression is row normalized (Red = high expression, Blue = Low expression).

(B) Leave-one-out cross-validation demonstrates that a robust model can be developed using these samples. Samples are plotted with confidence intervals based upon the predicted probability of the sample having a CD15$^+$ signature (y-axis) and the metagene score from binary regression during leave-one-out cross-validation. Blue numbers (1-6) represent CD15$^-$ samples, red numbers (7-12) represent CD15$^+$ samples. Numbers are placed at the probability value, and vertical lines indicate 95% confidence intervals. Dashed horizontal line indicates 50% probability.

(C) Probability of being scored as CD15$^+$ based on gene signature (y-axis) for independent samples sorted based upon CD15 staining (Blue circles, CD15$^+$ cells; red circles, CD15$^-$ cells; horizontal lines, mean probability for CD15$^+$ and CD15$^-$ samples).

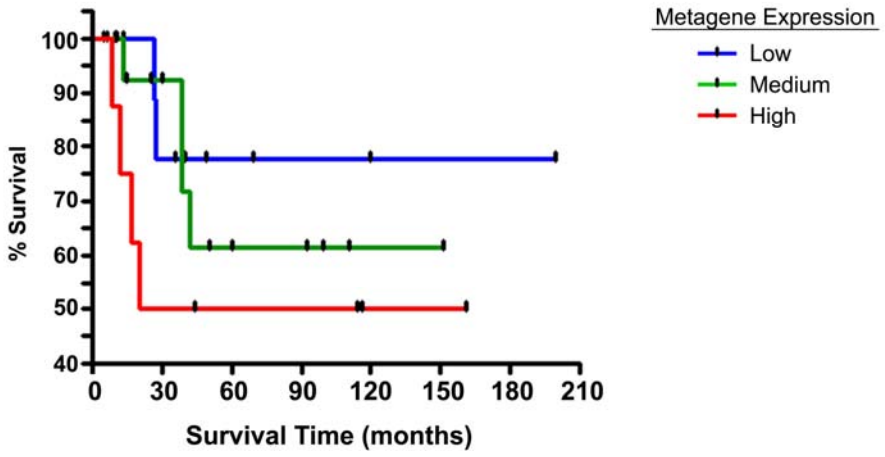

Figure S7. CD15$^+$ Gene Signature Predicts Survival in a Cohort of Medulloblastoma Patients

Kaplan-Meier plot of survival for patients with tumors having high (≥0.67, red line), medium (0.66-0.33, green line) or low (<0.33, blue line) probability of the CD15$^+$ signature. Black tick marks are surviving patients at time of last follow up. Log rank for trend p = 0.16.